Journal of Nuclear Materials 386–388 (2009) 67–70

Contents lists available at ScienceDirect

Journal of Nuclear Materials

journal homepage: www.elsevier.com/locate/jnucmat

Interaction between dislocations in bcc iron at high temperature

S.P. Fitzgerald *, S.L. Dudarev

EURATOM/UKAEA Fusion Association, Culham Science Centre, Abingdon, OX14 3DB, UK

A B S T R A C T

When a crystal deforms plastically, sources within, such as the Frank–Read source, emit dislocations, which then glide in response to the applied stress. As the dislocations move away from the source, they may encounter an obstacle, for example a grain boundary, impurity atom or locked dislocation, which they cannot overcome. As more dislocations are emitted, they 'pile up' near the obstacle, until their own stress fields acting back on the source prevent more dislocations from being produced, unless the external applied stress is increased. The properties of these pile-ups strongly influence the deformation of the crystal as a whole giving rise to the Hall–Petch effect [E. Hall, Proc. Phys. Soc. B 64 (1951) 747–753, N. Petch, J. Iron and Steel Institute 173 (1953) 25–28.] relating yield strength to grain size. In this paper we investigate how the observed strong variation of elastic constants as functions of temperature affects the strength of interactions between dislocations, and mechanisms of plastic deformation of iron at elevated temperatures. We find that the observed severe softening of the tetragonal shear modulus C' at high temperature gives rise to a drastic reduction in the repulsion between parallel like edge dislocations, and hence to a greatly increased number of dislocations in pile-ups, especially those in the $\langle 100\rangle\{001\}$ configuration. The associated increase in plastic strain will lead in turn to a conspicuous reduction in tensile strength as C' falls. The phenomenon is inherently anisotropic, and this work underlines the importance of including anisotropic elastic effects when modelling Fe at high temperatures.

1. Introduction

Crystalline bcc iron has cubic symmetry, and its elastic constant tensor is characterized by three independent parameters C_{11}, C_{12} and C_{44} which appear in Hooke's law:

$$\sigma_{mn} = C_{mnip}(C_{11}, C_{12}, C_{44})u_{ip}, \quad (1)$$

where σ and u are the stress and strain tensors respectively. Material properties are encoded in linear combinations of these fundamental parameters, for example the bulk modulus $B = (C_{11} + 2C_{12})/3$ and two independent shear moduli, C_{44} and $C' = (C_{11} - C_{12})/2$, describing the crystal's resistance to trigonal and tetragonal shear respectively. If elastic isotropy is assumed, these two shear moduli are taken equal, and only two remaining parameters are required to characterize the elastic properties of the crystal. Fig. 1 shows the variation with temperature of the elastic constants C_{11} and C_{12}, the bulk modulus B and the two independent shear moduli [1]. Even at room temperature, the two shear moduli are far from equal, and the discrepancy grows with temperature. Crucially, the C' modulus exhibits an extreme softening as the temperature approaches that of the α–γ phase transition. This experimentally observed behaviour agrees in principle with model calculations by Hasegawa et al. [2,3]. These calculations actually show C' reaching zero at the Curie temperature, which results from the approximation used (mean-field one-lattice-site treatment). Softening at the Curie point is a precursor to the structural phase transition, and the data show a deviation from smooth behaviour above around 750 °C. The α–γ transition is displacive, and naively one expects the shear modulus in the direction conducive to the transition to vanish there. In practice, thermal fluctuations and the volume-per-atom difference between the phases drive the lattice over the effective energy barrier to the γ phase, and C' need not actually reach zero.

In the next section we demonstrate the importance of elastic anisotropy of bcc iron by considering the phonon spectrum at elevated temperature, and comparing the results of anisotropic elasticity theory with those of the isotropic approximation. In subsequent sections we investigate the effect of anisotropy on dislocation interaction energies and pile-ups [4–6], and in the final section we apply an extension [7] of the analysis of [6] to Fe at high temperature, which gives an expression to estimate the plastic displacement occurring during the equilibriation of a Frank–Read source.

2. Phonons and the soft mode

A complementary description of the elastic behaviour of a solid is given by its phonon frequencies. These are determined by solving the elastic wave equations

* Corresponding author.
E-mail address: Steve.Fitzgerald@ukaea.org.uk (S.P. Fitzgerald).

0022-3115/$ - see front matter © 2009 Published by Elsevier B.V.
doi:10.1016/j.jnucmat.2008.12.304

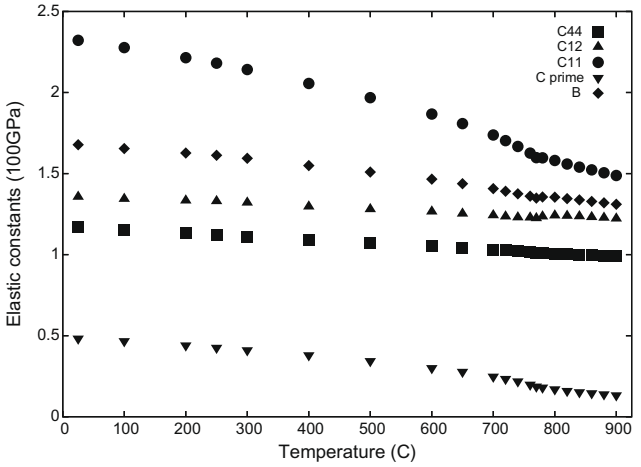

Fig. 1. Elastic moduli of single crystal α-Fe. Experimental data points are taken from Ref. [1]. The bulk modulus B and the trigonal shear modulus C_{44} remain significantly above zero, but the tetragonal shear modulus C' becomes close to zero at high temperatures. Isotropic elasticity does not distinguish the two moduli C_{44} and C', and is clearly a poor approximation to the true elastic behaviour of Fe at these temperatures.

$$\rho\frac{\partial^2 u_i}{\partial t^2} = C_{ijkl}\frac{\partial^2 u_k}{\partial x_j \partial x_l} \tag{2}$$

for the displacement vector u_k, where ρ is the mass density of the material. Plane wave solutions $\boldsymbol{u} = \boldsymbol{e}\exp i[\boldsymbol{k}\cdot\boldsymbol{x} - \omega t]$ satisfy the eigenvalue equation

$$[-\rho\omega^2\delta_{ik} + C_{ijkl}k_j k_l]e_k = 0, \tag{3}$$

prescribing the frequencies ω in terms of the wavevector $\boldsymbol{k}$, the elastic moduli C and the mass density ρ ($\boldsymbol{e}$ is the polarization vector). Fig. 2 shows the values taken by the three solutions for $\rho\omega^2$ in iron at 25 °C, 900 °C, and the isotropic approximation obtained by setting $C' = C_{44}$ at 900 °C. In the isotropic approximation the phonon frequencies are independent of the direction of $\boldsymbol{k}$, and two of the frequencies are degenerate, corresponding to the two transverse phonon modes. When anisotropy is taken into account, the clear distinction between the transverse and longitudinal modes can no longer be made. Moreover, a pronounced directionality is expressed, which becomes more extreme with increasing temperature. As the transition temperature is approached, frequencies corresponding to displacements in certain directions (⟨1 1 0⟩-type) tend towards zero, indicating the emergence of a *soft mode* [3]. In the limit, displacements in these directions can be effected at no energy cost. This is inherently anisotropic behaviour, and although the large-scale *elastic* properties of a polycrystalline sample could still be treated as isotropic, by averaging over grain orientations, the *plastic* evolution of microstructure occurs within single grains, and hence must be treated using full anisotropic elasticity.

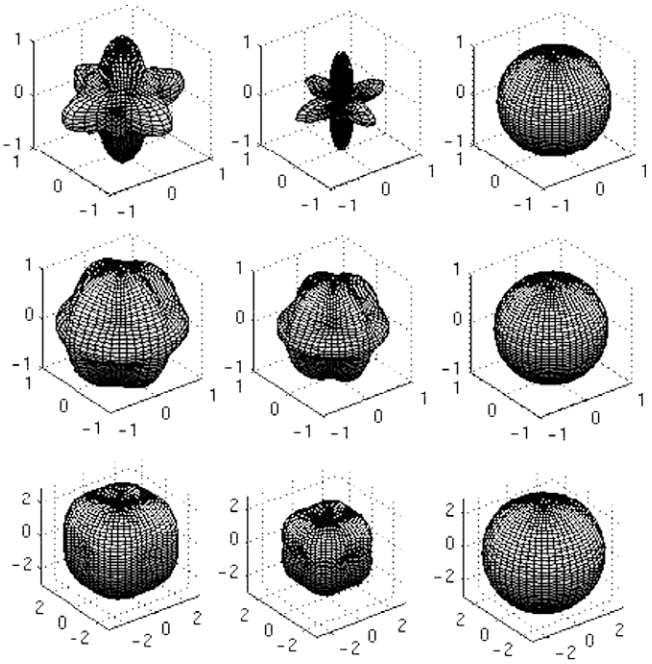

Fig. 2. Surfaces representing phonon frequency-squared $\rho\omega^2$ as a function of wavevector direction. Top to bottom: the three independent eigenvalues; left to right: 25 °C, 900 °C, and the isotropic approximation at 900 °C.

3. Elastic fields of straight dislocations

A general expression for the (two-dimensional) strain field at $\boldsymbol{r}$ created by an infinite straight dislocation passing through the origin is [8]:

$$u_{ip} = \frac{b_s}{2\pi|\boldsymbol{r}|}[-M_p S_{is} + N_p (NN)^{-1}_{ik}\{4\pi B_{ks} + (NM)_{kr}S_{rs}\}]; \tag{4}$$

where $\boldsymbol{r}$ is the vector from the dislocation to the field point at which the stress is evaluated, $\boldsymbol{b}$ is the dislocation's Burgers' vector, $\boldsymbol{M} = \boldsymbol{r}/|\boldsymbol{r}|$ and $\boldsymbol{N} = \boldsymbol{t}\wedge\boldsymbol{M}$. The bracketed quantities are defined as

$$(AB)_{jk} = c_{ijkl}A_i B_l, \tag{5}$$

for any two vectors A, B, and the two matrices B and S depend only the elastic constants and the line direction $\boldsymbol{t}$ (see [7,8]). The stress field σ_{mn} follows from Hooke's law (1). The hydrostatic pressure is given by $-\mathrm{Tr}(\sigma_{mn})/3$, and is shown in Fig. 3 for a ⟨1 0 0⟩(0 0 1)-type edge dislocation in iron at 900 °C. The circles predicted by the isotropic approximation are shown in each case for comparison. The differences are striking: when anisotropic effects are included, a local minimum appears at the position of the maximum pressure as calculated in the isotropic approximation. Also note the small regions of inverted pressure in the anisotropic case.

The elastic strain energy of two similar parallel edge dislocations may also be computed from elasticity theory:

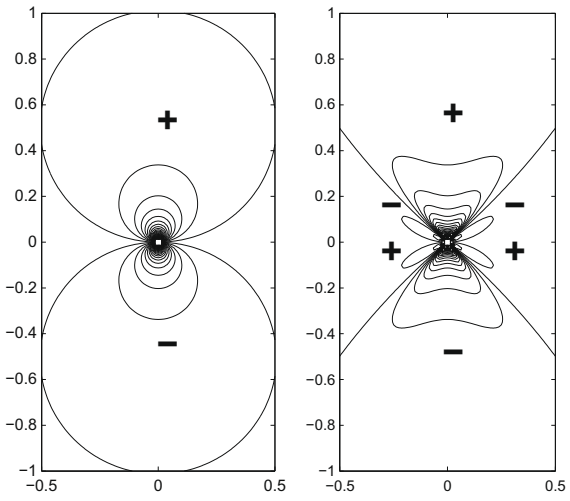

Fig. 3. Hydrostatic pressure fields surrounding a long straight ⟨1 0 0⟩-type edge dislocation in Fe at 900 °C (right). Left: isotropic calculation (arbitrary units). Regions of positive and negative pressure are indicated.

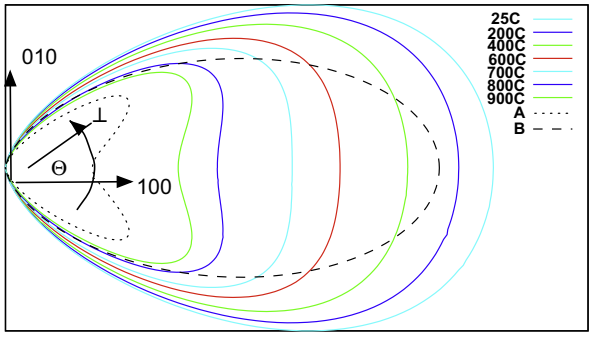

Fig. 4. Contours of equal angular interaction energy between two like parallel ⟨100⟩-type edge dislocations in Fe (dislocation lines into page; source dislocation fixed at extreme left, contours represent field dislocation moving between $\theta = \mp\pi/2$ at fixed separation.). Outermost solid curve 25 °C, to innermost solid curve 900 °C (arbitrary units). Dashed curves see text. (For interpretation of the references to colour in this figure legend, the reader is referred to the web version of this article.).

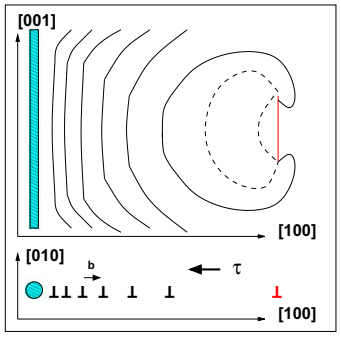

Fig. 5. Top: A Frank-Read source emitting dislocations into a pile-up. The shaded box represents the obstacle, and the red (lighter) segment is the source. Intermediate configurations are shown as dashed lines. Bottom: A side-on view showing the dislocations' common Burgers' vector and the direction in which the applied stress acts. (For interpretation of the references to colour in this figure legend, the reader is referred to the web version of this article.).

$$E = \frac{1}{2}\int \sigma_{ij}^{\text{total}} u_{ij}^{\text{total}} \mathrm{d}V = \frac{1}{2}\int (\sigma_{ij}^{1} + \sigma_{ij}^{2})(u_{ij}^{1} + u_{ij}^{2})\mathrm{d}V, \tag{6}$$

where the integral is taken over the entirety of the body. The diagonal terms in the product represent the elastic self-energies, whilst the two cross terms correspond to the interaction energy. Since the stress and strain fields are proportional to $1/r$, the total energy contains a logarithmic singularity corresponding to an inner cutoff near the dislocation core, where linear elasticity does not apply, and a term proportional to the logarithm of the size of the body. These may both be absorbed into the self-energies, and the interaction energy is well-behaved. It separates into a term depending only on the dislocations' separation, and one depending only on their relative angular orientation, which is shown in Fig. 4, for two ⟨100⟩(001) dislocations. One dislocation is located at the extreme left of the plot, whilst the other moves around a semicircle from the positive to negative y axis (the energy is symmetric in x). The curve marked A shows the result when the elastic constants take an 'extreme' value, with very low C' ($C_{12} = 1.22$, $C_{44} = 0.900$, $C' = 0.06$). The curve marked B was calculated using these adjusted constants, but with C_{44} and C' replaced by their average, corresponding to the isotropic approximation. The disparity between these curves indicates the failure of isotropic elasticity: in no way can the anisotropic interaction effects be accounted for by averaging over orientations. By considering all directions as equivalent, the isotropic approximation fails to capture the effect of the modulus C' sharply falling toward zero. The position of minimum interaction energy is the same in both cases, namely that where the separation vector of the two dislocations is orthogonal to their Burgers' vector. This configuration allows for the most effective cancellation of the pressure fields, with the area of greatest positive pressure due to one dislocation aligned with that of greatest negative pressure due to the other. However, the configuration of maximal interaction energy as calculated in the isotropic approximation, corresponding to the dislocations sharing a common slip plane, becomes a local minimum once anisotropic effects are included. At high temperatures the discrepancy can reach a factor of five. This is directly related to the softening of C', and has important consequences for the plastic behaviour of iron and iron-based steels and alloys.

4. Dislocation pile-ups

As mentioned in the introduction, similar dislocations gliding under stress on a common glide plane pile up when the leading dislocation approaches an obstacle it cannot overcome. The dislocations' mutual repulsion ensures that the array does not collapse, and this provides the crystal's resistance to further deformation. An analytical model developed in 1951 [6] quantitatively describes the elastic and geometric properties of pile-ups in terms of the applied stress magnitude τ_0 and a parameter A, which encodes the magnitude of the inter-dislocation force:

$$f = \frac{A}{|\boldsymbol{r}|}. \tag{7}$$

If n like parallel dislocations are piled up against a similar dislocation locked at the origin (Fig. 5), we can define an nth order polynomial $g(x)$ such that its roots coincide with the positions of the dislocations:

$$g(x) = (x - x_1)(x - x_2)\ldots(x - x_n). \tag{8}$$

Differentiating ln$g$ gives

$$\frac{g'(x)}{g(x)} = \sum_{i=1}^{n} \frac{1}{x - x_i} = \frac{\text{total force at } x}{A}. \tag{9}$$

Subtracting the force due to the jth dislocation, setting $x = x_j$ and adding the forces A/x_j and τ_0 due to the immobile dislocation at the origin and the applied stress respectively, we arrive at the following equilibrium conditions to be satisfied at each x_j:

$$g(x_j) = 0; A\lim_{x\to x_j}\left(\frac{g'(x)}{g(x)} - \frac{1}{x - x_j}\right) + \frac{A}{x_j} - \tau_0 = 0. \tag{10}$$

These correspond to the differential equation

$$Axg'' + 2g'(A - \tau_0 x) + Axq(n,x)g = 0, \tag{11}$$

where q must be chosen so that there is an nth order polynomial solution for $g(x)$. If we take $q = n/x$ and rescale x into units where $A = 2\tau_0$, it becomes the associated Laguerre equation with parameter 1, and the dislocations' positions are given by

$$\{x_i\} = \frac{A}{2\tau_0}\{p_i\}, \tag{12}$$

where $\{p_i\}$ are the n roots of the first derivative of the $(n+1)$th Laguerre polynomial. Clearly, increasing the applied stress or reducing the inter-dislocation force causes the pile-up to compress more, and vice versa.

The parameter A may be determined by comparing the above definition with the expression obtained from the Peach–Koehler formula [9] for the force on a dislocation with line element $\boldsymbol{t}$, Burgers' vector $\boldsymbol{b}$ in *any* stress field $\boldsymbol{\sigma}$:

$$\boldsymbol{f}_{\text{PK}} = \boldsymbol{t} \wedge (\boldsymbol{\sigma}\cdot\boldsymbol{b}). \tag{13}$$

Using the expression for the stress field experienced by a dislocation '1' at $\boldsymbol{r}$, due a dislocation '2' situated at $\boldsymbol{r}'$ gives

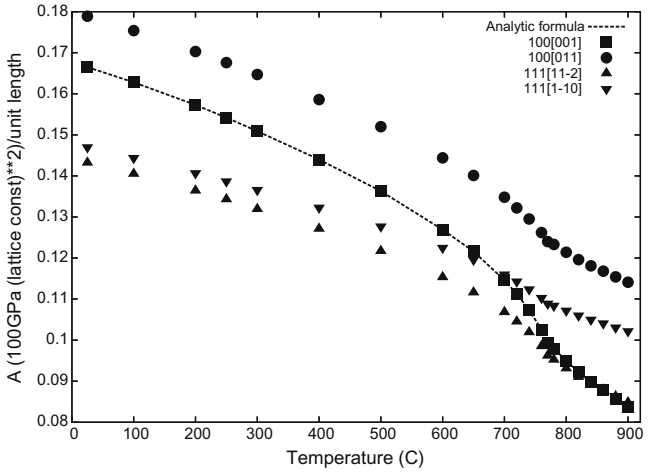

Fig. 6. Values taken by the inter-dislocation force parameter for the four principle dislocation configurations in bcc iron vs. temperature.

$$\boldsymbol{f}^{12} = \boldsymbol{t}^{1} \wedge (\boldsymbol{\sigma}^{2}(\boldsymbol{r} - \boldsymbol{r}') \cdot \boldsymbol{b}^{1}), \tag{14}$$

which in general has a component in both glide and climb directions. Since we are considering only glide, we may select this component and identify A.

In general, A cannot be computed explicitly, since the integrals in the definition of the matrices S and B [8] must be evaluated numerically. However in the $\langle 100\rangle(001)$ case the result is

$$\begin{aligned} A_{100} &= \frac{C_{12}+C'}{4\pi}\sqrt{\frac{C_{44}C'}{(C_{12}+C_{44}+C')(C_{12}+2C')}} \\ &\approx \frac{\sqrt{C'}}{4\pi}\sqrt{\frac{C_{12}C_{44}}{C_{12}+C_{44}}} \quad \text{at small} C'. \end{aligned} \tag{15}$$

At high temperatures, A_{100} is proportional to $\sqrt{C'}$, since C_{12} and C_{44} both vary slowly with temperature, while C' decreases sharply as the temperature approaches that of the phase transition. The variation with temperature of the values taken by A for the four main dislocation configurations in bcc iron is shown in Fig. 6. The relative magnitude of A for the various configurations behaves in the same way as the straight dislocation strain energy, calculated in [10]. They all decrease with temperature, with the $\langle 100\rangle(001)$ falling the most steeply by virtue of its $\sqrt{C'}$ dependence. For the pile-up, this translates into a reducing resistance to compression at a given applied stress, especially for the $100(001)$ and $111(11\bar{2})$ orientations. Indeed, if C' were to reach zero, the $\langle 100\rangle(001)$ pile-up would collapse completely. In the isotropic approximation $C' \to C_{44}$

$$A_{100} \to \frac{C_{44}}{4\pi}\frac{C_{12}+C_{44}}{C_{12}+2C_{44}}, \tag{16}$$

and the high-temperature collapse is overlooked.

5. Equilibriation of sources and plastic displacement

The authors [7] recently extended the model of [6] to quantify the plastic displacement occurring during the equilibriation of a dislocation source. Since the Frank–Read source can be thought of as a segment of dislocation line pinned at both ends, we can regard the source as another dislocation with the same Burgers' vector as the others (a typical source has initial length of order $10^4 b$, so this treatment is reasonable) and use the same solution as in the previous section. The solution for n mobile dislocations is now $g = L'_{n+2}$, and the positions are given as before by the scaled zeros of g. There are $n+1$ zeros in the above, the first n of which are the equilibrium coordinates of the mobile dislocations, and the greatest root is the position of the source, which is by definition fixed at some x_0 (related to the grain size or average obstacle spacing), so for given A, we can find a consistent relation between the imposed force τ_0 and n. Furthermore, we can determine the total plastic displacement d at a given τ_0 by summing the distances travelled by the n dislocations from the source to their equilibrium positions, with the result [7]

$$\begin{aligned} d &\approx \frac{3|\boldsymbol{b}|x_0\tau_0}{8A} \quad \text{or} \\ \tau_0 &\propto \frac{Ad}{|\boldsymbol{b}|x_0} \end{aligned} \tag{17}$$

if the plastic displacement is specified. The second line indicates that the applied stress required to produce a given plastic displacement is proportional to A, and hence for a pile-up of $\langle 100\rangle(001)$-type dislocations, to $\sqrt{C'}$. If C' were to reach zero, the plastic displacement at any applied stress would be infinite, corresponding to the collapse of the crystal (as would a zero shear modulus alone). This behaviour is of course unphysical, since the phase transition intervenes and Fe remains solid until its melting point.

The behaviour of the A parameters (Fig. 6) indicates that the tensile strength of iron, defined by some critical value of the plastic strain, is expected to fall sharply above around 700 °C. This behaviour has been observed in ferritic-martensitic steels, see for example Ref. [11].

Acknowledgement

The authors gratefully acknowledge helpful discussions with Professor R. Bullough and Professor D.J. Bacon. This work was supported by the UK Engineering and Physical Sciences Research Council, by EURATOM, and by EXTREMAT integrated project under contract number NMP3-CT-2004-500253.

References

[1] D. Dever, J. Appl. Phys. 43 (8) (1972) 3293.
[2] H. Hasegawa, M.W. Finnis, D.G. Pettifor, J. Phys. F: Met. Phys. 15 (1985) 19.
[3] H. Hasegawa, M.W. Finnis, D.G. Pettifor, J. Phys. F: Met. Phys. 55 (1987) 2049.
[4] E. Hall, Proc. Phys. Soc. B 64 (1951) 747.
[5] N. Petch, J. Iron and Steel Institute 173 (1953) 25–28.
[6] J. Eshelby, F. Frank, F. Nabarro, Phil. Mag. 42 (1951) 351.
[7] S.P. Fitzgerald, S.L. Dudarev, Proc. Roy. Soc. Lond. A 464 (2008) 2549–2559.
[8] D. Bacon, D. Barnett, R. Scattergood, Prog. Mater. Sci. 23 (1980) 51.
[9] M. Peach, J.S. Koehler, Phys. Rev. 80 (3) (1950) 436, doi:10.1103/PhysRev.80.436.
[10] S.L. Dudarev, R. Bullough, P. Derlet, Phys. Rev. Lett. 100 (2008) 135503.
[11] S.J. Zinkle, Phys. Plasmas 12 (2005) 058101.